

Post Common Envelope Binaries from SDSS - III. Seven new orbital periods

A. Rebassa-Mansergas¹, B. T. Gänsicke¹, M.R. Schreiber², J. Southworth¹,
A.D. Schwope³, A. Nebot Gomez-Moran³, A. Aungwerojwit^{4,1}, P. Rodríguez-Gil^{5,6},
V. Karamanavis⁷, M. Krumpel³, E. Tremou⁷, R. Schwarz³, A. Staude³, J. Vogel³

¹ *Department of Physics, University of Warwick, Coventry CV4 7AL, UK*

² *Departamento de Física y Astronomía, Universidad de Valparaíso, Avenida Gran Bretaña 1111, Valparaíso, Chile*

³ *Astrophysikalisches Inst. Potsdam, An der Sternwarte 16, 14482, Potsdam, Germany*

⁴ *Department of Physics, Faculty of Science, Naresuan University, Phitsanulok, 65000, Thailand*

⁵ *Isaac Newton Group of Telescopes, Apdo. de Correos 321, E-38700, Santa Cruz de La Palma, Spain*

⁶ *Instituto de Astrofísica de Canarias, Vía Láctea, s/n, La Laguna, E-38205, Tenerife, Spain*

⁷ *Dept. of Physics, Sect. of Astrophysics, Astronomy & Mechanics, Univ. of Thessaloniki, 541 24 Thessaloniki, Greece*

Accepted 2008. Received 2008; in original form 2008

ABSTRACT

We present follow-up spectroscopy and photometry of 11 post common envelope binary (PCEB) candidates identified from multiple Sloan Digital Sky Survey (SDSS) spectroscopy in an earlier paper. Radial velocity measurements using the Na I $\lambda\lambda$ 8183.27, 8194.81 absorption doublet were performed for nine of these systems and provided measurements of six orbital periods in the range $P_{\text{orb}} = 2.7 - 17.4$ h. Three PCEB candidates did not show significant radial velocity variations in the follow-up data, and we discuss the implications for the use of SDSS spectroscopy alone to identify PCEBs. Differential photometry confirmed one of our spectroscopic orbital periods and provided one additional P_{orb} measurement. Binary parameters are estimated for the seven objects for which we have measured the orbital period and the radial velocity amplitude of the low-mass companion star, K_{sec} . So far, we have published nine SDSS PCEBs orbital periods, all of them $P_{\text{orb}} < 1$ d. We perform Monte-Carlo simulations and show that 3σ SDSS radial velocity variations should still be detectable for systems in the orbital period range of $P_{\text{orb}} \sim 1 - 10$ days. Consequently, our results suggest that the number of PCEBs decreases considerably for $P_{\text{orb}} > 1$ day, and that during the common envelope phase the orbital energy of the binary star is maybe less efficiently used to expell the envelope than frequently assumed.

Key words: Binaries: spectroscopic – stars:low-mass – stars: white dwarfs – binaries: close – stars: post-AGB – stars: evolution variables

1 INTRODUCTION

Most of the stellar sources are formed as parts of binary or multiple systems. Therefore the study of binary star evolution represents an important part of studying stellar evolution. While the majority of the wide main sequence binaries evolve as if they were single stars and never interact, a small fraction are believed to undergo mass transfer interactions. Once the more massive main sequence star becomes a red giant it eventually overfills its Roche lobe. Dynamically unstable mass transfer exceeding the Eddington limit ensues onto the companion star, which consequently also overfills its own Roche lobe. The two stars then orbit inside a common envelope (CE, e.g. Paczynski 1976; Livio & Soker 1988;

Iben & Livio 1993; Taam & Ricker 2006; Webbink 2007), and friction inside this envelope causes a rapid decrease of the binary separation. Orbital energy and angular momentum are extracted from the binary orbit and lead to the ejection of the envelope, exposing a post common envelope binary (PCEB). After the envelope is expelled PCEBs keep on evolving towards shorter orbital periods through angular momentum loss via gravitational radiation and, for companion stars above the fully convective mass limit, by magnetic wind braking. In binaries that do not undergo a CE phase both components evolve almost like single stars and keep their wide binary separations. A predicted consequence is hence a strongly bi-modal binary separation and

orbital period distribution among post-main sequence binaries, with PCEBs concentrated at short orbital periods, and non-PCEBs at long orbital periods.

The scenario outlined above is thought to be a fundamental formation channel for a wide range of astronomical objects such as low-mass X-ray binaries, double degenerate white dwarfs, neutron star binaries, cataclysmic variables and super-soft X-ray sources. Some of these objects will eventually end their lives as type Ia supernovae and short gamma-ray bursts, which are of great importance for cosmological studies.

While the basic scenario of CE evolution has been known for a long time (e.g. Paczynski 1976), the physical details involved are complex and still poorly understood. As a result, full hydrodynamical models for the CE phase have been calculated only for a small number of cases (Sandquist et al. 2000; Ricker & Taam 2008). Similarly, orbital evolution through magnetic braking is not well understood, with different prescriptions in angular momentum loss differing by orders of magnitudes (e.g. Verbunt & Zwaan 1981; Andronov et al. 2003). Consequently, current binary population synthesis models still have to rely on simple parametrisations of energy or angular momentum equations (Nelemans et al. 2000; Dewi & Tauris 2000; Nelemans & Tout 2005; Politano & Weiler 2006, 2007).

A fundamental problem in advancing our understanding of CE evolution and magnetic braking in close binaries is the shortage of stringent observational constraints that can be used to test and calibrate the theory. PCEBs consisting of a white dwarf and a main sequence star are a very well-suited class of objects to provide the required innovative observational input since they are numerous, well understood in terms of their stellar components, they are bright and hence accessible with 2–8 metre telescopes, and their study is not complicated by mass transfer. Schreiber & Gänsicke (2003) analysed a sample of 30 well studied PCEBs and showed that the population of PCEBs known so far is not only small but also heavily biased towards young systems with low-mass secondary stars, and can hence not be used for comparison with population models (e.g. Willems & Kolb 2004).

The Sloan Digital Sky Survey (York et al. 2000; Stoughton et al. 2002; Adelman-McCarthy et al. 2008, SDSS) is currently dramatically increasing the number of known white dwarf plus main sequence (WDMS) binaries (Silvestri et al. 2007; Schreiber et al. 2007), paving the way for large-scale observational PCEB population studies. We have initiated an observational programme to identify the PCEBs among the SDSS WDMS binaries, and to determine their binary parameters (Rebassa-Mansergas et al. 2007; Schreiber et al. 2008). Those systems in which significant radial velocity variation is detected, are classified as close binaries or PCEBs. Here we present follow-up observations of 11 PCEB candidates identified in Rebassa-Mansergas et al. (2007) and provide accurate values of the orbital periods as well as estimates of their stellar parameters and orbital inclinations for seven of these systems.

2 OBSERVATIONS

We have obtained time-resolved spectroscopy and photometry for 11 SDSS WDMS binaries (Table 1, Fig. 1), henceforth designated SDSS J0052–0053, SDSS J0246+0041, SDSS J0309–0101, SDSS J0820+4314, SDSS J0314–0111, SDSS J1138–0011, SDSS J1151–0007, SDSS J1529+0020, SDSS J1724+5620, SDSS J2241+0027 and SDSS J2339–0020. Below we briefly describe the instrumentation used for the observations, and outline the reduction of the data.

2.1 Spectroscopy

(i) *Magellan-Baade*. Intermediate-resolution long-slit spectroscopy of SDSS J0314–0111 and SDSS J2241+0027 was obtained on the nights of 2007 October 2 and 3 using the IMACS imaging spectrograph attached to the Magellan Baade telescope at Las Campanas Observatory. The $600 \ell \text{mm}^{-1}$ red-sensitive grating was used along with the slit-view camera and a slit width of 0.75 arcsec, giving a reciprocal dispersion of 0.39 \AA px^{-1} . The IMACS detector is a mosaic of eight $2\text{k} \times 4\text{k}$ SiTe CCDs, and long-slit spectra with this instrument are spread over the short axis of four of these CCDs. Using a grating tilt of 14.7° allowed us to position the $\text{Na I } \lambda\lambda 8183.27, 8194.81$ doublet towards the centre of CCD2 and the $\text{H}\alpha$ line near the centre of CCD4.

The images were reduced using STARLINK software, and the PAMELA and MOLLY packages (Marsh 1989) were employed to optimally extract and calibrate the spectra. By fitting Gaussian functions to arc and sky emission lines we find that the spectra have a resolution of approximately 1.6 \AA . Helium arc lamp exposures were taken at the start of each night in order to derive a wavelength solution with a statistical uncertainty of only 0.002 \AA (Marsh et al. 1994). This was applied to each spectrum taken on the same night. Detector flexure was measured and removed from the wavelength solution for each spectrum using the positions of sky emission lines (Southworth et al. 2006; Schreiber et al. 2008). Flux calibration and telluric line removal was performed using MOLLY and spectra of the standard star BD +28°4211.

(ii) *Magellan-Clay and Very Large Telescope (VLT)*. The observations of SDSS J1138–0011, SDSS J1151–0007 and SDSS J1529+0020 were obtained with the same setup and reduced in the same manner as described by Schreiber et al. (2008), and we refer the reader to that paper for full details.

(iii) *New Technology Telescope (NTT)*. Two observing runs were carried out at the NTT in August and October 2007, providing intermediate time-resolved spectroscopy of SDSS J0052–0053, SDSS J0246+0041, SDSS J0309–0101, SDSS J2241+0027 and SDSS J2339–0020. We used the EMMI spectrograph equipped with the Grating#7 grating, the MIT/LL red mosaic detector, and a 1 arcsec wide long-slit, resulting in a wavelength coverage of $\lambda 7770 - 8830 \text{ \AA}$. The data were bias-corrected and flat-fielded using the STARLINK software, and spectra were optimally extracted using the PAMELA package. Helium-Agon arc lamp spectra were taken at the beginning of each night and were then used to establish a generic pixel-wavelength relation using MOLLY. Specifically, we fitted a fourth order polynomial which gave rms smaller than 0.02 \AA for all spectra. We then used the night sky emission lines to adjust the zero-point of the wavelength

Table 1. Log of the observations. Included are the target names, the SDSS *ugriz* psf-magnitudes, the period of the observations, the telescope/instrument setup, the exposure time, and the number of exposures.

Spectroscopy											
SDSS J	<i>u</i>	<i>g</i>	<i>r</i>	<i>i</i>	<i>z</i>	Dates	Telesc.	Spectr.	Grating/Grism	Exp.[s]	# spec.
005245.11–005337.2	20.47	19.86	19.15	17.97	17.22	16/08/07-20/08/07	NTT	EMMI	Grat#7	1200	21
024642.55+004137.2	19.99	19.23	18.42	17.29	16.60	05/10/07-09/10/07	NTT	EMMI	Grat#7	650-800	19
030904.82–010100.8	20.77	20.24	19.50	18.43	17.77	07/10/07-12/10/07	NTT	EMMI	Grat#7	1500	4
031404.98–011136.6	20.78	19.88	19.03	17.76	16.98	02/10/07-03/10/07	M-Baade	IMACS	600 line/mm	600-900	12
113800.35–001144.4	19.14	18.86	18.87	18.15	17.53	16/08/06-23/03/07	VLT (<i>sm</i>)	FORS2	1028z	900	2
						18/06/07-23/06/07	WHT	ISIS	158R	1500	1
						17/05/07-20/05/07	M-Clay	LDSS-3	VPH-red	500-600	5
115156.94–000725.4	18.64	18.12	18.14	17.82	17.31	17/05/07-20/05/07	M-Clay	LDSS-3	VPH-red	450-600	17
152933.25+002031.2	18.69	18.20	18.33	17.98	17.48	18/05/07-20/05/07	M-Clay	LDSS-3	VPH-red	500-1000	18
172406.14+562003.0	15.83	16.03	16.42	16.42	16.52	25/09/00-29/03/01	SDSS			900	23
224139.02+002710.9	19.62	18.82	18.40	17.33	16.58	02/10/07-03/10/07	M-Baade	IMACS	600 line/mm	600	2
						07/10/07-12/10/07	NTT	EMMI	Grat#7	750-800	3
233928.35–002040.0	20.40	19.68	19.15	18.07	17.36	07/10/07-12/10/07	NTT	EMMI	Grat#7	1400-1700	15
Photometry											
SDSS J	<i>u</i>	<i>g</i>	<i>r</i>	<i>i</i>	<i>z</i>	Dates	Telesc.		Filter band	Exp.[s]	# hrs
031404.98–011136.6	20.78	19.88	19.03	17.76	16.98	19/09/06-20/09/06	CA 2.2 m		clear	35-60	10.3
082022.02+431411.0	15.92	15.85	16.11	15.83	15.38	21/11/06-24/11/06	Kryoneri 1.2 m		<i>R</i>	60	8.2
172406.14+562003.0	15.83	16.03	16.42	16.42	16.52	04/08/06-10/08/06	IAC80		<i>I</i>	80-180	12.2
						25/03/06-13/09/06	AIP 70 cm		<i>R</i>	60-90	55.6

Notes: M-Baade and M-Clay refer to the two Magellan telescopes at Las Campanas observatory. We use *sm* to indicate that the data were taken in service mode. CA 2.2 is the 2.2 metre telescope at Calar Alto observatory.

calibration, thus correcting for instrument flexure. The spectral resolution of our instrumental setup determined from the sky lines is 2.8\AA . Finally, the spectra were calibrated and corrected for telluric absorption within MOLLY using observations of the standard star Feige 110.

(iv) *William Herschel Telescope (WHT)*. One spectrum of SDSS J1138-0011 was taken with the 4.2 m William Herschel Telescope in June 2007 at the Roque de los Muchachos observatory on La Palma. The double-beam ISIS spectrograph was equipped with the R158R and the R300B gratings, and a 1 arcsec long-slit, providing a wavelength coverage of $\lambda 7600 - 9000\text{\AA}$. The spectral resolution measured from the sky lines is 1.6\AA . Reduction and calibration were carried in the same way as described for the NTT above.

(v) *SDSS*. For one system, SDSS J1724+5620, we were able to determine an accurate orbital period from our photometry alone, but were lacking follow-up spectroscopy. SDSS DR6 contains three 1-d calibrated spectra for SDSS J1724+5620 (MJD-PLT-FIB 51813-357-579, 51818-358-318, and 51997-367-564). Each of these spectra is combined from at least 3 individual exposures of 900 s, which are also individually released as part of DR6¹. For SDSS J1724+5620, a total of 23 sub-spectra are available, of which 22 allowed reliable radial velocity measurements.

2.2 Photometry

(i) *IAC80 and AIP 70 cm telescopes*. We obtained differential photometry of SDSS J1724+5620 with the IAC80 telescope at the Observatorio del Teide (Spain) and the 70 cm telescope of the Astrophysical Institute of Potsdam at Babels-

berg (Germany) for a total of 13 nights during May, August and September 2006 and March 2007. The IAC80 cm telescope was equipped with a $2k \times 2k$ CCD. A binning factor of 2 was applied in both spatial directions and only a region of 270×270 (binned) pixels of size 0.66 arcsec was read. The detector used at the Babelsberg 70 cm telescope was a cryogenic $1k \times 1k$ Tek CCD. The whole frame was read with a binning factor of 3, resulting in a scale of 1.41 arcsec/pixel . A semiautomated pipeline involving DoPHOT was used to reduce the images and extract the photometric information.

(ii) *Calar Alto 2.2 m telescope*. We used CAFOS with the SiTe $2k \times 2k$ pixel CCD camera on the 2.2 metre telescope at the Calar Alto observatory to obtain filter-less differential photometry of SDSS J0314-0111. Only a small part of the CCD was read out in order to improve the time resolution. The data were reduced using the pipeline described in Gänsicke et al. (2004), which pre-processes the raw images in MIDAS and extracts aperture photometry using the SEXTRACTOR (Bertin & Arnouts 1996).

(iii) *Kryoneri 1.2 m telescope*. Filter-less photometry of SDSS J0820+4311 was obtained in November 2006 at the 1.2 m Kryoneri telescope using a Photometrics SI-502 516×516 pixel camera. The data reduction was carried out in the same way as described above for the Calar Alto observations.

3 ORBITAL PERIODS

3.1 Radial Velocities

In Rebassa-Mansergas et al. (2007) we measured the radial velocities fitting a second order polynomial plus a double-Gaussian line profile of fixed separation to the Na I $\lambda\lambda 8183.27, 8194.81$ absorption doublet. Free parameters

¹ <http://www.sdss.org/dr6/dm/flatFiles/spCFrame.html>

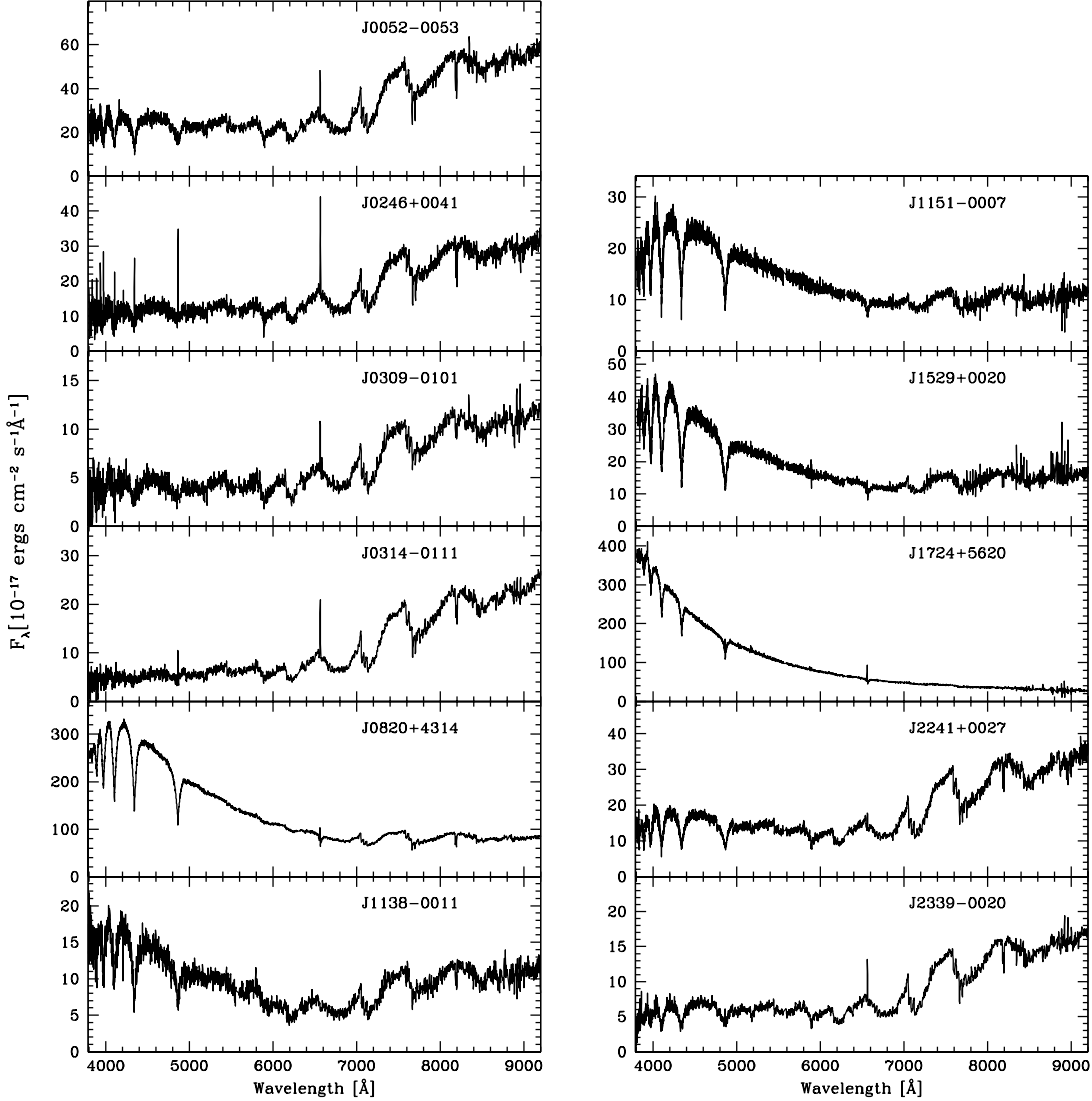


Figure 1. SDSS spectra of the 11 SDSS white dwarf main sequence binaries studied in this work.

were the amplitude and the width of each Gaussian and the radial velocity of the combined doublet. Here we adopt a slightly modified approach, using just a single width parameter for both line components. This reduction in the number of free parameters increases the robustness of the fits. Radial velocities measured in this way for nine WDMS binaries are given in Table 2. In addition, we measured the companion star radial velocities for SDSS J1724+5620 by means of a Gaussian fit to the H α emission line clearly visible in 22 of the SDSS sub-exposures (Sect. 2.1), which are also reported in Table 2.

Scargle (1982) periodograms calculated from the radial velocities of each system to investigate the periodic nature of the velocity variations contain a number of aliases due to the sampling pattern of the observations (Fig. 2, left panel). We carried out sine-fits of the form

$$V_r = K_{\text{sec}} \sin \left[\frac{2\pi(t - T_0)}{P_{\text{orb}}} \right] + \gamma \quad (1)$$

to the velocity data sets of each system, where γ is the systemic velocity, K_{sec} is the radial velocity semi-amplitude of the companion star, T_0 is the time of inferior conjunction of the secondary star, and P_{orb} is the orbital period. Several fits were done, adopting the frequencies corresponding to the strongest peaks in the power spectra as initial conditions. The parameters resulting from these fits are reported in Table 3. For SDSS J0052-0053, SDSS J0246+0041, SDSS J0314-0111, SDSS J1151-0007, SDSS J1529+0020 and SDSS J2339-0020 the sine-fits allow a unique choice of the orbital period. For SDSS J1724+5620, the sampling of the SDSS spectra is very sparse, resulting in finely structured aliases superimposed on a sequence of large aliases spaced by 1 d^{-1} . A sine fit to the radial velocities started off at the 3 d^{-1} alias provides a spectroscopic orbital period of $7.99243(16) \text{ h}$, which is consistent with the more accurate value determined from the photometry (Sect. 3.2). The radial velocity data for all seven systems folded over their orbital periods are shown in Fig. 2 (right panel).

Table 2. Radial velocities measured from the Na I $\lambda\lambda 8183.27, 8194.81$ doublet, except for SDSS J1724+5620, where radial velocities measured from the H α emission line in the 15 min SDSS-subspectra are given. Note that the provided HJD is the resulted from HJD-2400000.

HJD	RV [km s ⁻¹]	HJD	RV [km s ⁻¹]	HJD	RV [km s ⁻¹]	HJD	RV [km s ⁻¹]	HJD	RV [km s ⁻¹]
SDSS J0052-0053		54379.8169	106.6 \pm 7.4	SDSS J1138-0011		54238.7778	59.7 \pm 11.3	51993.9263	-81.3 \pm 10.7
54328.7467	42.5 \pm 18.7	54379.8622	42.5 \pm 14.5	54205.5902	-12.8 \pm 5.7	54238.8109	-156.4 \pm 11.2	51993.9387	-101.9 \pm 10.4
54328.7933	-15.0 \pm 13.6	54380.8165	-97.1 \pm 9.9	54207.7340	-7.7 \pm 12.6	54238.8270	-160.8 \pm 32.7	51993.9511	-111.0 \pm 11.4
54328.8077	-40.7 \pm 13.7	54380.8372	-92.3 \pm 8.2	54237.5647	-13.9 \pm 11.6	54238.8372	-188.3 \pm 14.9	51994.9683	-127.4 \pm 10.6
54328.8825	31.5 \pm 27.5	54380.8762	-85.7 \pm 7.8	54237.5721	5.1 \pm 10.3	54239.5635	157.9 \pm 9.9	51994.9805	-130.2 \pm 10.5
54328.8969	-4.0 \pm 9.9	54380.8842	-72.9 \pm 8.0	54238.4936	9.9 \pm 9.6	54239.6756	-121.3 \pm 8.0	51994.9928	-131.6 \pm 12.5
54329.6885	31.5 \pm 9.3	54381.6121	-63.7 \pm 12.7	54238.5352	-5.1 \pm 8.5	54240.5548	202.6 \pm 21.2	51997.9480	-106.9 \pm 10.6
54329.7028	-12.1 \pm 11.8	54381.7427	77.3 \pm 7.6	54238.6889	23.1 \pm 10.6	54240.6338	-182.8 \pm 7.8	51997.9602	-132.0 \pm 10.8
54329.7172	-50.9 \pm 16.4	54381.8122	126.4 \pm 8.0	54271.3996	9.2 \pm 6.7	54240.6844	28.9 \pm 10.1	51997.9724	-136.1 \pm 11.4
54329.8269	-56.1 \pm 14.1	54381.8958	157.2 \pm 8.4	SDSS J1151-0007		54240.7296	204.4 \pm 8.7	SDSS J2241+0027	
54329.8412	-60.8 \pm 13.4	54382.8362	-31.9 \pm 8.9	54237.5904	48.4 \pm 14.9	54240.7357	194.9 \pm 7.9	54376.5842	2.6 \pm 14.0
54329.8556	-55.3 \pm 14.8	54385.7884	-71.1 \pm 11.5	54237.5976	129.3 \pm 11.4	54240.7417	175.1 \pm 9.5	54377.5637	6.6 \pm 6.6
54330.7154	29.7 \pm 10.8	SDSS J0309-0101		54238.5245	-147.6 \pm 13.0	54240.8311	-114.7 \pm 8.1	54378.5290	13.2 \pm 9.9
54330.7298	-30.8 \pm 12.3	54381.6726	60.4 \pm 12.4	54238.5709	-81.0 \pm 11.6	54240.8372	-87.6 \pm 9.9	54379.5523	39.9 \pm 13.3
54330.7441	-59.7 \pm 16.0	54381.7714	31.5 \pm 12.0	54238.7012	-160.1 \pm 6.9	54240.8432	-54.6 \pm 12.7	54382.5261	-20.1 \pm 17.7
54330.8136	56.8 \pm 17.7	54381.8386	41.0 \pm 10.7	54239.5084	-129.0 \pm 7.7	54240.8498	8.4 \pm 31.7	SDSS J2339-0020	
54330.8279	28.2 \pm 9.3	54382.8626	51.7 \pm 15.9	54239.6047	233.4 \pm 8.0	SDSS J1724+5620		54380.5088	-25.3 \pm 13.4
54330.8423	-29.3 \pm 12.2	SDSS J0314-0111		54239.6602	-175.8 \pm 9.8	51812.6531	133.8 \pm 13.2	54380.5511	3.7 \pm 8.2
54330.9158	32.6 \pm 14.1	SDSS J0314-0111		54240.4793	148.4 \pm 11.7	51812.6531	133.8 \pm 13.2	54381.5526	-116.1 \pm 9.2
54332.7313	22.7 \pm 11.1	54376.7386	-54.6 \pm 8.2	54240.5236	-227.1 \pm 12.5	51812.6656	114.2 \pm 12.2	54382.5097	11.7 \pm 10.2
54332.7457	59.3 \pm 23.5	54376.7862	-151.3 \pm 8.5	54240.5291	-207.4 \pm 11.5	51813.5993	60.8 \pm 25.2	54382.5869	94.2 \pm 9.2
54332.8433	23.1 \pm 9.6	54376.8051	-116.1 \pm 11.4	54240.5346	-198.2 \pm 8.5	51813.6161	77.2 \pm 17.1	54382.6866	86.1 \pm 10.0
SDSS J0246+0041		54376.8581	64.5 \pm 10.8	54240.5400	-163.8 \pm 9.5	51813.6284	132.0 \pm 11.4	54382.7587	24.2 \pm 9.1
54378.6386	-127.5 \pm 11.4	54376.8996	174.7 \pm 30.0	54240.6033	219.8 \pm 11.4	51813.6425	118.3 \pm 12.3	54383.5274	-134.4 \pm 11.2
54378.6496	-122.7 \pm 13.0	54377.6572	119.8 \pm 8.0	54240.6088	220.5 \pm 9.3	51813.6631	121.1 \pm 11.1	54385.5605	-181.3 \pm 17.0
54378.7955	18.3 \pm 8.8	54377.6830	186.1 \pm 9.3	54240.6142	161.2 \pm 10.1	51813.6768	103.2 \pm 10.6	54385.6462	-177.3 \pm 9.0
54379.6704	176.9 \pm 11.3	54377.7380	164.5 \pm 8.0	54240.6197	111.7 \pm 9.3	51813.6889	94.1 \pm 10.7	54385.6663	-164.9 \pm 23.9
54379.6789	159.0 \pm 15.6	54377.7782	-2.6 \pm 7.5	SDSS J1529+0020		51818.5877	71.7 \pm 22.8	54385.6864	-133.4 \pm 12.8
54379.6875	177.3 \pm 9.7	54377.8165	-116.1 \pm 9.5	54238.6219	-3.3 \pm 23.9	51818.6178	109.6 \pm 13.0	54385.7065	-104.0 \pm 21.6
54379.7813	132.6 \pm 7.9	54377.8672	-98.9 \pm 8.1	54238.6795	-145.1 \pm 11.7	51818.6297	122.4 \pm 13.9	54385.7495	-49.8 \pm 27.1
		54377.8866	-44.3 \pm 12.1			51818.6418	127.4 \pm 13.2	54385.7696	-16.9 \pm 9.8

The periodograms calculated from the radial velocity measurements of the PCEB candidates SDSS J0309-0101, SDSS J1138-0011, and SDSS J2241+0027 do not reveal any significant peak. The low amplitude of the radial velocity variations observed in these three objects suggests that they may be wide WDMS binaries rather than PCEBs. This issue will be discussed further in Sect. 5.3.

3.2 Light curves

The light curves of SDSS J0314-0111 and SDSS J1724+5620 display variability with an amplitude of ~ 0.05 mag and ~ 0.1 mag, respectively. We calculated periodograms for both systems using the `ORT/TSA` command in `MIDAS`, which folds and phase-bins the data using a grid of trial periods and fits a series of Fourier terms to the folded light curve (Schwarzenberg-Czerny 1996).

A strong peak is found in the periodogram of SDSS J0314-0111 at 3.8 d^{-1} , i.e. 6.3 h (Fig. 3, top left panel). Folding the photometric data over that period results in a double-humped modulation which we identify as ellipsoidal modulation (Fig. 3, middle left panel). The detection of ellipsoidal modulation indicates that the companion star must

be filling a significant amount of its Roche-lobe radius and have a moderately high inclination, both of which hypothesis are confirmed below in Sect. 4. The two minima differ in depth, as expected for ellipsoidal modulation because of the stronger gravity darkening on the hemisphere facing the white dwarf. The two maxima are also unequal, which is observed relatively often in PCEBs, and thought to be related to the presence of star spots (e.g. Kawka & Vennes 2003; Tappert et al. 2007). We conclude that the strongest periodicity detected in the photometry of SDSS J0314-0111 is consistent with the spectroscopic orbital period (Table 3). As the radial velocities span a longer temporal baseline than the photometry, they provide the more accurate period measurement, and we adopt $P_{\text{orb}} = 6.319 \pm 0.015 \text{ h}$ for SDSS J0314-0111.

For the analysis of SDSS J1724+5620 we separately merged the data for the *R* and *I* band, normalised both data sets to their respective mean values, and finally combined all data into a single data set. The `ORT` periodogram calculated from the full light curve displays a strong signal at 3 d^{-1} , with weak aliases related to the sampling pattern inherent to the data (Fig. 3, top right panel). Given the large quasi-sinusoidal shape of the modulation, and the high effec-

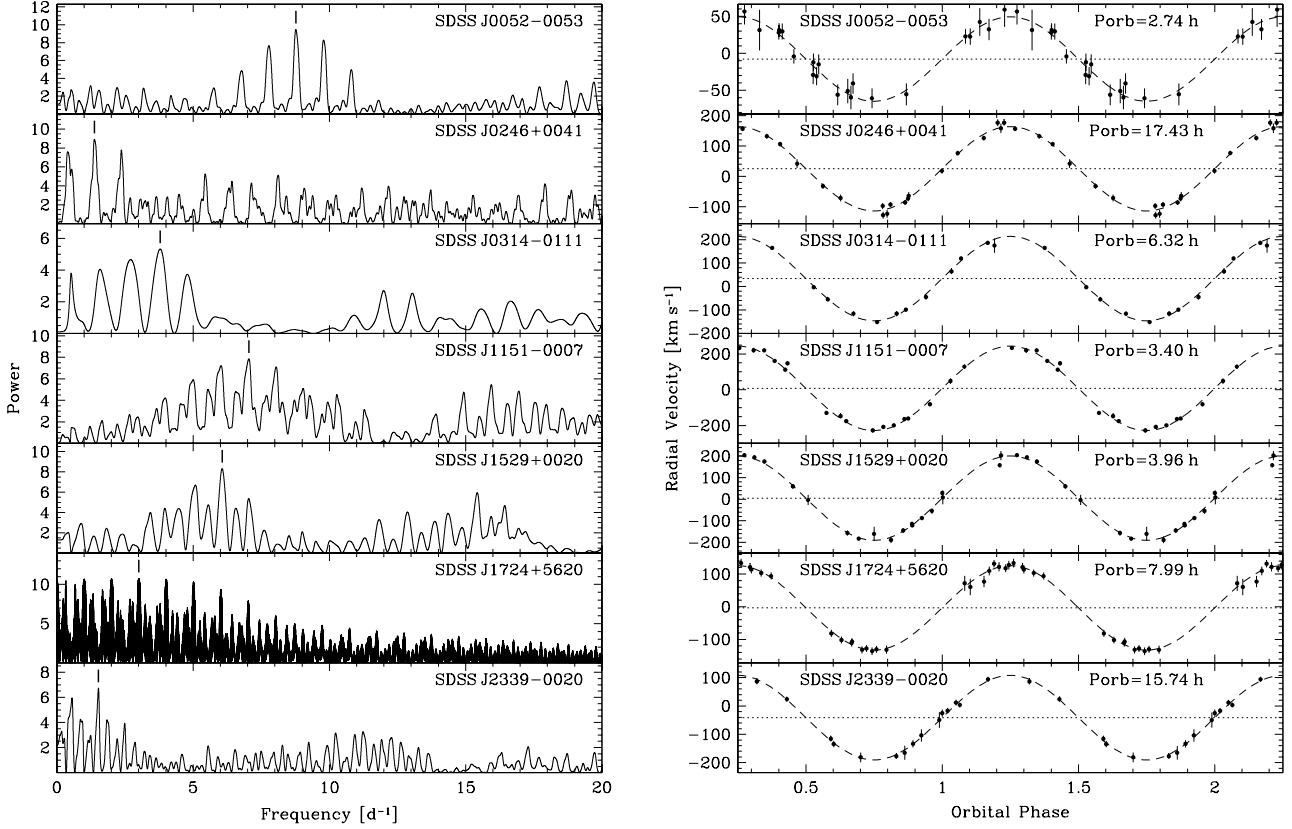


Figure 2. Left: Scargle periodograms calculated from the radial velocity variations measured from the NaI absorption doublet in SDSS J0052-0053, SDSS J0246+0041, SDSS J0314-0111, SDSS J1151-0007, SDSS J1529+0020, and SDSS J2339-0020, and from the $\text{H}\alpha$ emission line in SDSS J1724+5620. The aliases with the highest power are indicated by tick marks. Right: the radial velocity measurements folded over the orbital periods of the systems, as determined from the best sine fits (Table 3).

tive temperature of the white dwarf (Table 4), we identify the observed photometric variability as being due to heating effect (or reflection effect as it is often referred to in the literature). A sine fit to the combined data (dashed line) provided the following photometric ephemeris

$$\text{HJD}(\phi = 0) = 2453865.29(1) + E \times 0.3330193(13), \quad (2)$$

where $\phi = 0$ refers to the occurrence of minimum light. The photometric period of 8 h is consistent with the alias pattern in the periodogram calculated from the $\text{H}\alpha$ radial velocity variations (Fig. 2, left panel). The phase-folded light curve using the photometric period is shown on the middle right hand panel of Fig. 3. Based on the above ephemeris, the accumulated phase error for the first SDSS subspectrum (Table 2) is 0.024 cycles, which is sufficiently good to phase the radial velocities obtained from the SDSS spectra with Eq. (2). The phase-folded light curve and radial velocity curve are shown in Fig. 4. The phase offset between the two curves is 0.226 ± 0.005 , which is consistent with $\simeq 0.25$ within the error of the fit and the ephemeris. A 0.25 phase offset is what is expected from the assumption that the photometric modulation is related to a heating effect, i.e. maximum light and red-to-blue crossing of the radial velocity corresponds to the superior conjunction of the secondary star, whereas minimum light and blue-to-red crossing of the radial velocity corresponds to its inferior conjunction.

Finally, we show in the bottom panel of Fig. 3 a 3.5

hours light curve of SDSS J0820+4314. We monitored the system through a total of 8.2 hours on three different nights (see Table 1), and found no significant photometric modulation. This implies that the companion star is significantly under-filling its Roche lobe and/or that the binary inclination is very low. The orbital period of the system will hence need to be measured from a radial velocity study.

4 BINARY PARAMETERS

In Rebassa-Mansergas et al. (2007) we developed a spectral decomposing/fitting technique for the analysis of WDMS binaries with SDSS spectroscopy. In brief, this analysis determines the white dwarf effective temperature, surface gravity, mass and radius, the spectral type and radius of the main sequence companion, as well as two independent distance estimates based on the properties of the two stellar components. Given that the SDSS spectra reduction pipeline has been improved with DR6 (Adelman-McCarthy et al. 2008), we have re-analysed here the seven PCEBs for which we were able to determine orbital periods. Comparison with the results from DR5 reported in Rebassa-Mansergas et al. (2007) shows that the fit parameters differ slightly, but agree in the vast majority of cases within the errors. We report the average stellar parameters determined from fits to the multiple

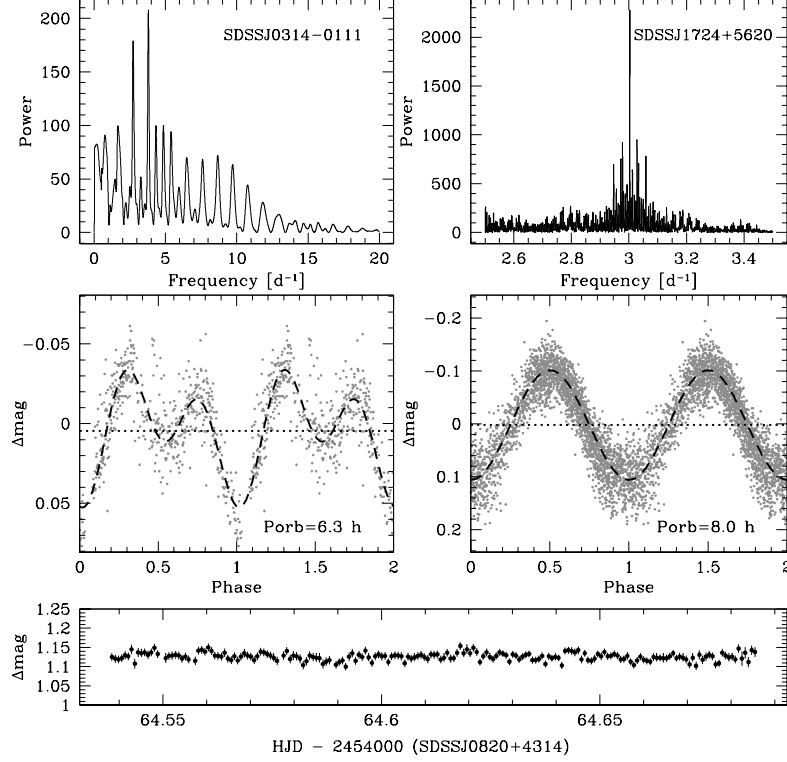


Figure 3. Top and middle panels: ORT periodograms and light curves folded on strongest photometric periodicities, $P_{\text{orb}} = 6.32 \pm 0.02$ h for SDSS J0314-0111 and $P_{\text{orb}} = 7.99246 \pm 0.00003$ h for SDSS J1724+5620. Bottom panel: the light curve of SDSS J0820+4314 is essentially flat, and a periodogram calculated from this data does not contain any significant periodicity.

SDSS spectra in Table 4. Rewriting Kepler’s third law (assuming common notation),

$$\frac{(M_{\text{wd}} \sin i)^3}{(M_{\text{wd}} + M_{\text{sec}})^2} = \frac{P_{\text{orb}} K_{\text{sec}}^3}{2\pi G} \quad (3)$$

as

$$\sin i = \frac{K_{\text{sec}}}{M_{\text{wd}}} \left(\frac{P_{\text{orb}}}{2\pi G} \right)^{1/3} (M_{\text{wd}} + M_{\text{sec}})^{2/3}, \quad (4)$$

and adopting the orbital period determined from the analysis of the radial velocities and the photometry, as well as the masses from the analysis of the SDSS spectra, we are now able to estimate the orbital inclinations for the seven systems in Table 4. Two systems require some additional notes: SDSS J0314-0111 contains a DC white dwarf, and hence no white dwarf parameters could be determined from the spectral analysis, and we assume $M_{\text{wd}} = 0.65 M_{\odot}$ for the estimate of the inclination. In SDSS J1724+5620 the hot white dwarf is irradiating the companion star, and the implications are discussed in more detail in Sect. 5.2.

Inspecting Eq.(4), it is clear that the dominant uncertainties in the inclination estimates are only M_{wd} and M_{sec} , as the orbital periods and K_{sec} velocities are accurately determined. The primary uncertainty in the inclination estimates is M_{sec} , as it is based on the spectral type of the companion star, adopting the spectral type-mass-radius relation given by Rebassa-Mansergas et al. (2007). M_{wd} is determined from fitting the Balmer line profiles, and relatively

well constrained. Given that $\sin i \propto M_{\text{sec}}^{2/3}$, but $\sin i \propto M_{\text{wd}}$, the relative weight of the uncertainty in M_{sec} is alleviated. We estimate the uncertainties on the binary inclinations in Table 4 by assuming in Eq.(4) the range in M_{sec} implied by a spectral type uncertainty of ± 0.5 spectral classes plus the associated errors in the spectral type-mass relation, as well as the range in M_{wd} resulting from the Balmer line profile fits. Given the high estimate for the binary inclination, SDSS J1529+0020 is a good candidate for photometric follow-up observations probing for eclipses in its light curve.

In addition, knowing that $M_{\text{sec}}/M_{\text{wd}} = K_{\text{wd}}/K_{\text{sec}} = q$, we can also estimate the expected orbital velocity of the white dwarf K_{wd} (Table 4). The predicted K_{wd} amplitudes could easily be measured, e.g. using *HST/COS* observations, and such measurements would be very valuable to improve the overall constraints on the system parameters of these PCEBs. Finally, we can estimate the orbital separations and Roche lobe radii of the secondary stars from Kepler’s third law and Eggleton’s (1983) expression

$$R_{\text{Lsec}} = \frac{a 0.49 q^{2/3}}{0.6 q^{2/3} + \ln(1 + q^{1/3})} \quad (5)$$

Table 4. Average binary parameters obtained for the seven PCEBs which have orbital period and K_{sec} measurements. M_{wd} , M_{sec} , R_{sec} , spectral type, T_{eff} and $\log g$ are obtained following Rebassa-Mansergas et al. (2007), except for SDSS J0314–0111, where we assume a WD mass of $0.65 \pm 0.1 M_{\odot}$ (see text for details). P_{orb} and K_{sec} are measured in Sect. 3 of this work. Estimates of orbital separations a , q , K_{wd} , secondary Roche lobe radius R_{Lsec} and inclinations are obtained from the equations given in Sect. 4. SDSS J1724+5620 is a particular case, as the inner hemisphere of the companion is irradiated. Constraints on its orbital parameters are obtained assuming a spectral type between M3-5, and considering different $K_{\text{sec,corr}}$ values for each mass and radius (see Sect. 5.2). An additional constraint for its inclination comes from the fact that SDSS J1724+5620 is not eclipsing.

	SDSS J0052–0053	SDSS J0246+0041	SDSS J0314–0111	SDSS J1151–0007	SDSS J1529+0020	SDSS J1724+5620	SDSS J2339–0020
$M_{\text{wd}}[M_{\odot}]$	1.2 ± 0.4	0.9 ± 0.2	0.65 ± 0.1	0.6 ± 0.1	0.40 ± 0.04	0.42 ± 0.01	0.8 ± 0.4
$M_{\text{sec}}[M_{\odot}]$	0.32 ± 0.09	0.38 ± 0.07	0.32 ± 0.09	0.19 ± 0.08	0.25 ± 0.12	$\sim 0.25 - 0.38$	0.32 ± 0.09
q	0.3 ± 0.1	0.4 ± 0.1	0.5 ± 0.2	0.3 ± 0.2	0.6 ± 0.3	$\sim 0.6 - 0.9$	0.4 ± 0.2
$a[R_{\odot}]$	1.1 ± 0.1	3.7 ± 0.2	1.7 ± 0.1	1.0 ± 0.1	1.1 ± 0.1	$\sim 1.8 - 1.9$	3.3 ± 0.4
$P_{\text{orb}}[\text{h}]$	2.735 ± 0.002	17.43 ± 0.04	6.32 ± 0.02	3.399 ± 0.003	3.962 ± 0.003	$7.992463(3)$	15.74 ± 0.02
$K_{\text{sec}}[\text{km s}^{-1}]$	57 ± 3	141 ± 4	175 ± 5	234 ± 8	193 ± 5	$\sim 129 - 214$	150 ± 4
$K_{\text{wd}}[\text{km s}^{-1}]$	15 ± 6	59 ± 15	86 ± 28	79 ± 38	123 ± 61	$\sim 78 - 194$	57 ± 29
Sp_{sec}	4 ± 0.5	3 ± 0.5	4 ± 0.5	6 ± 0.5	5 ± 0.5	$3 - 5$	4 ± 0.5
$R_{\text{sec}}[R_{\odot}]$	0.33 ± 0.10	0.39 ± 0.08	0.33 ± 0.10	0.19 ± 0.10	0.26 ± 0.13	$\sim 0.26 - 0.39$	0.33 ± 0.10
$R_{\text{sec}}/R_{\text{Lsec}}$	1.0 ± 0.6	0.3 ± 0.1	0.6 ± 0.2	0.6 ± 0.5	0.7 ± 0.5	$\sim 0.4 - 0.6$	0.3 ± 0.1
$i[^\circ]$	8 ± 1	51 ± 7	53 ± 8	56 ± 11	70 ± 22	$\gtrsim 50^\circ, \lesssim 75^\circ$	53 ± 18
$T_{\text{eff}}[\text{k}]$	16100 ± 4400	16600 ± 1600	—	10400 ± 200	14100 ± 500	35800 ± 300	13300 ± 2800
$\log g$	9.0 ± 0.7	8.5 ± 0.3	—	8.0 ± 0.2	7.6 ± 0.1	7.40 ± 0.05	8.4 ± 0.7

Table 3. Orbital periods, semi-amplitudes K_{sec} , systemic velocities γ_{sec} , and reduced χ^2 from sine fits to the Na I doublet radial velocity data for the strongest two to three aliases in the periodograms shown in Fig. 2. The best-fit values are set in bold. The SDSS H α radial velocities of SDSS J1724+5620 are folded on the photometric orbital period obtained in Sect. 3.2 (which is more accurate than the spectroscopically determined value of the orbital period). Note also that the semi-amplitude measurement of this system is underestimated, as it comes from RV measurements of H α emission from the irradiated face of the companion (see Sect. 5.2).

System	P_{orb} [h]	K_{sec} [km s $^{-1}$]	γ_{sec} [km s $^{-1}$]	χ^2_{red}
SDSS J0052–0053	3.0850 ± 0.0090	47.2 ± 6.6	-2.9 ± 5.8	3.74
	2.7350 ± 0.0023	57.0 ± 3.1	-7.2 ± 2.6	0.50
	2.4513 ± 0.0035	54.8 ± 5.8	-9.1 ± 4.6	1.96
SDSS J0246+0041	61.1 ± 2.7	124 ± 17	16 ± 12	20.3
	17.432 ± 0.036	140.7 ± 3.5	24.9 ± 2.7	1.25
	10.130 ± 0.031	163 ± 16	34 ± 10	21.8
SDSS J0314–0111	8.66 ± 0.17	154 ± 19	44 ± 16	27.1
	6.319 ± 0.015	174.9 ± 4.8	31.0 ± 3.4	1.15
	3.979 ± 0.013	202 ± 20	-2 ± 16	34.4
SDSS J1151–0007	3.3987 ± 0.0027	233.8 ± 8.1	9.0 ± 5.9	3.55
	2.9849 ± 0.0092	213 ± 22	-22 ± 23	64.7
	4.759 ± 0.028	171 ± 18	11 ± 14	26.9
SDSS J1529+0020	3.9624 ± 0.0033	193.1 ± 5.2	6.0 ± 4.1	1.92
	1.5558 ± 0.0024	182 ± 21	6 ± 15	36.7
	$7.992463(31)$	129.3 ± 1.9	-3.5 ± 1.8	0.41
SDSS J1724+5620	43.18 ± 0.78	121 ± 18	-50 ± 15	13.5
SDSS J2339–0020	15.744 ± 0.016	149.8 ± 4.0	-40.9 ± 2.6	0.69

5 NOTES ON INDIVIDUAL SYSTEMS

5.1 SDSS J0052–0053, a detached CV in the period gap?

SDSS J0052–0053 has the shortest orbital period, the smallest radial velocity amplitude, and lowest inclination in our sample (Fig. 2, Table 4). Another intriguing feature of SDSS J0052–0053 is that the Roche lobe secondary radius and the secondary star radius overlap within the errors (see Table 4). The SDSS and Magellan spectra certainly rule out ongoing mass transfer, i.e. that SDSS J0052–0053 is a disguised cataclysmic variable (CV). Two possible scenarios could apply to the system. SDSS J0052–0053 could be either be a pre-CV that is close to develop in a semi-detached configuration, or it could be a detached CV in the 2–3 h period gap. Standard evolution models based on the disrupted magnetic braking scenario (e.g. Rappaport et al. 1983; Kolb 1993; Howell et al. 2001) predict that CVs stop mass transfer and the secondary star shrinks below its Roche lobe radius once they evolve down to $P_{\text{orb}} \simeq 3$ h. Subsequently, these detached CVs evolve through the period gap, until the companion star fills its Roche lobe again at $P_{\text{orb}} \simeq 2$ h. Population models based on the disrupted magnetic braking hypothesis predict that the ratio of detached CVs to pre-CVs (with appropriate companion star masses to (re-)initiate mass transfer at $P_{\text{orb}} \simeq 2$ h) should be $\gtrsim 4$ (Davis et al. 2008), hence a substantial number of such systems is expected to exist. So far, only one other system with similar properties is known, HS 2237+8154 (Gänsicke et al. 2004).

5.2 SDSS J1724+5620, a PCEB with a strong heating effect

SDSS J1724+5620 contains the hottest white dwarf among our sample of PCEBs, which affects the determination of its system parameters in several ways. Firstly, irradiation

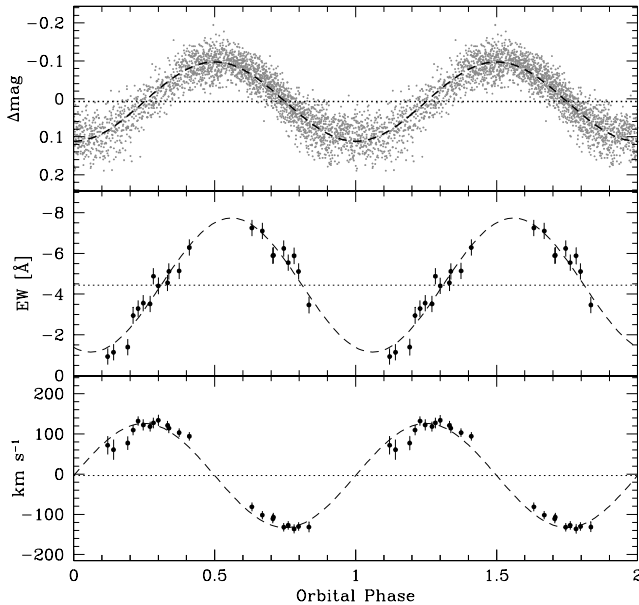


Figure 4. Top panel: The IAC80 and AIP 70 cm photometry of SDSS J1724+5620 folded over the photometric period of 7.9924632 ± 0.0000312 h. Middle pane: the equivalent width variation of the $H\alpha$ emission line measured from the SDSS spectra of SDSS J1724+5620 (Table 2) folded over the photometric period. Maximum equivalent width occur roughly in phase with the maximum in the light curve (see Sect. 5.2 for details). Bottom panel: the radial velocity variation of the $H\alpha$ emission line. The relative phasing with respect to the photometry is consistent with the photometric modulation being caused by irradiation of the secondary star by the hot white dwarf.

heating the inner hemisphere of the companion will cause it to appear of earlier spectral type than an unheated star of same mass. This effect is observed in the analysis of the three SDSS spectra available in DR6. The spectral decomposition types the companion star as M3-4, and combining the flux scaling factor of the M star template and the spectral type-radius relation (see Rebassa-Mansergas et al. 2007, for details) indicates an average distance of $d_{\text{sec}} = 633 \pm 144$ pc. This is roughly twice the distance implied from the model fit to the residual white dwarf spectrum, $d_{\text{wd}} = 354 \pm 15$ pc, indicating that the spectral type of the companion star determined from the SDSS spectrum is too early for its actual mass and radius, as expected for being heated by the white dwarf. Fixing the spectral type of the companion to M5, the spectral decomposition results in $d_{\text{sec}} = 330 \pm 150$ pc, consistent with the distance based on the white dwarf fit.

An additional complication is that the radial velocity of the companion star was measured from the $H\alpha$ emission line, as the Na I absorption doublet was too weak in the individual 900 s SDSS spectra. The equivalent width of the $H\alpha$ emission shows a noticeable variation as a function of binary phase, with maximum equivalent width near the maximum in the light curve, indicating that the $H\alpha$ emission is concentrated on the inner hemisphere of the companion star (Fig. 4). A phase offset of 0.046 ± 0.008 is observed between the photometry and the $H\alpha$ equivalent width, which we attribute to systematic problems in measuring the equivalent width of the $H\alpha$ embedded in the photospheric absorption line from the

white dwarf, given the poor quality of the individual SDSS subspectra. As a consequence of $H\alpha$ predominantly originating on the inner hemisphere of the companion star, the observed K_{sec} is an underestimate of the true radial velocity amplitude (e.g. Wade & Horne 1988; Orosz et al. 1999; Vennes et al. 1999; Aungwerojwit et al. 2007). The radial velocity amplitude of the secondary star’s centre of mass can be written as (Wade & Horne 1988):

$$K_{\text{sec,corr}} = \frac{K_{\text{sec}}}{1 - (1 + q)(\Delta R/a)}, \quad (6)$$

where ΔR is the displacement of the centre of light from the centre of mass. $\Delta R = 0$ implies that the centre of light and the centre of mass coincide, whilst $\Delta R = R_{\text{sec}}$ gives the maximum possible displacement. If one assumes that the irradiated emission on the secondary is distributed uniformly over the inner hemisphere, and that the contribution of the irradiation is zero on its un-irradiated face, then $\Delta R = (4/3\pi)R_{\text{sec}}$ (Wade & Horne 1988; Orosz et al. 1999; Vennes et al. 1999). Assuming that the spectral type is in the range M3–5, different combinations of secondary mass and radius, and radial velocity amplitude, $K_{\text{sec,corr}}$, can then constrain the orbital parameters of SDSS J1724+5620 (Table 4).

5.3 SDSS J0309-0101, SDSS J1138-0011 and SDSS J2241+0027: wide WDMS binaries?

SDSS J0309-0101, SDSS J1138-0011 and SDSS J2241+0027 were flagged as PCEB candidates by Rebassa-Mansergas et al. (2007) on the base of a 3σ radial velocity variation in between their different SDSS spectra, as measured from either the $H\alpha$ emission line or the Na I absorption doublet from the companion star. However, the additional intermediate-resolution spectra taken for these three objects (Table 1) do not show a significant radial velocity variation (Table 2, Fig. 5). It is therefore important to review the criterion that we used in our first paper to identify PCEBs from repeated SDSS spectroscopy in the light of two subtle changes.

On the one hand, we have slightly modified the procedure to fit the Na I absorption doublet, as outlined in Sect. 3.1. By comparing the Na I DR5 radial velocities in Rebassa-Mansergas et al. (2007) with those obtained with the new procedure for the same spectra, we find an average difference of 5 km s^{-1} with a maximum difference of 10.5 km s^{-1} . In all cases the measurements agree within the errors.

On the other hand, we were using DR5 spectra in Rebassa-Mansergas et al. (2007), but the analysis carried out here was done using DR6 spectra, which were processed with a different reduction pipeline (Adelman-McCarthy et al. 2008). A comparison between the DR5 and DR6 radial velocity values obtained in Rebassa-Mansergas et al. (2007) and in this work respectively (both measured following our new procedure) provides in this case an average difference of 6.5 km s^{-1} , with a maximum of 22 km s^{-1} . Again, the radial velocity measurements agree, with the exception of a single spectrum, within the errors.

The conclusion from comparing our two methods, and the two SDSS data releases, is that the radial velocity

Table 5. Parameters of the PCEBs derived from calculating their post-CE evolution according to Schreiber & Gänsicke (2003). t_{cool} and t_{sd} are the cooling age and the predicted time until the system enters the semi-detached CV phase respectively. P_{sd} denoted the zero-age CV orbital period while P_{CE} is the orbital period the system had when it left the CE phase. As discussed in the text and displayed in Fig 6, the predicted evolution depends sensitively on the mass and the radius of the secondary star, in particular as the errors of all estimated secondary masses overlap with the value assumed for the fully convective mass limit. We therefore give values for the both scenarios.

Name SDSS J	P_{orb} [days]	t_{cool} [years]	CMB			GR		
			P_{sd} [days]	P_{CE} [days]	t_{sd} [years]	P_{sd} [days]	P_{CE} [days]	t_{sd} [years]
0052-0053	0.114	4.2×10^8	0.125	0.46	0.0	0.114	0.145	0.0
0246+0041	0.726	3.1×10^8	0.146	0.78	1.1×10^9	0.113	0.73	8.1×10^{10}
0314-0111	0.263	—	0.12	—	3.7×10^7	0.11	—	6.2×10^9
1151-0007	0.142	5.0×10^8	0.12	0.55	2.7×10^6	0.07	0.15	1.8×10^9
1529+0020	0.165	1.3×10^8	0.11	0.41	4.7×10^6	0.10	0.17	2.5×10^9
1724+5620	0.333	3.2×10^6	0.12	0.34	6.1×10^7	0.11	0.33	1.7×10^{10}
2339-0020	0.656	5.1×10^8	0.12	0.74	1.0×10^9	0.11	0.66	6.5×10^{10}

measurements obtained are in general consistent within their errors. However, the offsets can be sufficient to move a given system either way across our criterion to identify PCEB candidates, being defined a 3σ radial variation between their SDSS spectra. This is specifically the case for systems with either low-amplitude radial velocity variations, or faint systems with noisy spectra. An additional note concerns the use of the $\text{H}\alpha$ line as probe for radial velocity variations. Rebassa-Mansergas et al. (2007) identified SDSS J2241+0027 as a PCEB candidate on the basis of a large change in the $\text{H}\alpha$ radial velocity between the two available SDSS spectra. However, the velocities obtained from the Na I doublet did not differ significantly. Inspecting the spectra again confirms the results of Rebassa-Mansergas et al. (2007). This suggests that the absorption lines from the secondary star are a more robust probe of its radial velocity.

A somewhat speculative explanation for the shifts found from $\text{H}\alpha$ radial velocity measurements is that the main sequence star is relatively rapidly rotating, and that the $\text{H}\alpha$ emission is patchy over its surface. A nice example of a this effect is the rapidly rotating ($P = 0.459$ d) active M-dwarf EY Dra, which displays $\text{H}\alpha$ radial velocity variations with a peak-to-peak amplitude of $\sim 100 \text{ km s}^{-1}$ (Eibe 1998). In order to explain the $\text{H}\alpha$ radial velocity shifts of a few 10 km s^{-1} observed in e.g. SDSS J2241+0027, the companion star should be rotating with a period of ~ 1 d. According to Cardini & Cassatella (2007), low-mass stars such as the companions in our PCEBs that are a few Gyr old are expected to have rotational periods of the order of tens of days, which is far too long to cause a significant $\text{H}\alpha$ radial velocity variation at the spectral resolution of the SDSS spectra. However, Cardini & Cassatella’s study was based on single stars, and the rotation rates of the companion stars in (wide) WDMS binaries is not well established.

6 PCEB EVOLUTION

Following Schreiber & Gänsicke (2003) we determine the cooling age and the future evolution of the new PCEBs. We assume classical and disrupted magnetic braking according to the standard theory of CV evolution (e.g.

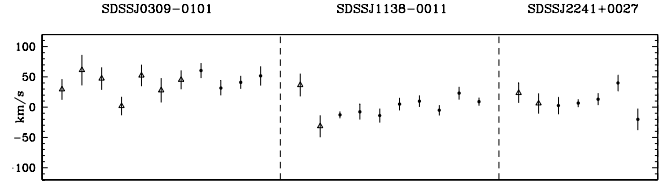


Figure 5. SDSS radial velocities (triangles) along with the Na I radial velocities measured in this work (solid dots) of SDSS J0309-0101, SDSS J1138-0011 and SDSS J2241+0027. The data at hand suggest that this three systems are wide WDMS binaries instead of PCEBs.

Verbunt & Zwaan 1981). We used the cooling tracks of Wood (1995) and find that most of the PCEBs left the CE about $1 - 5 \times 10^8$ years ago, the only exception being SDSS J1724+5620 which appears to be much younger. The time still needed to enter the semi-detached CV configuration is shorter than the Hubble time for all the systems, qualifying them as representatives for the progenitors of the current CV population. The numbers we obtained from the theoretical analysis are summarised in Table 5. The estimated secondary masses are generally very close to the fully convective boundary (for which we assume $M_{\text{cc}} = 0.3M_{\odot}$, see however the discussion by Mullan & MacDonald 2001 and Chabrier et al. 2007 on how this mass limit may be affected by magnetic activity) and the uncertainties involved in the secondary mass determination are quite large. The predicted evolution of all systems should therefore be considered highly uncertain as it is not clear whether magnetic braking applies or not. We therefore give in Table 5 the values obtained for both scenarios. The effect of not knowing whether magnetic braking or only gravitational radiation will drive the evolution of the systems is illustrated in Fig. 6, which shows the expected post CE evolution for SDSS J1152-0007 and SDSS J0246+0041 for both cases.

Inspecting Table 5, the case of SDSS J0052-0053 is particularly interesting. The estimated secondary radius is consistent with its Roche-lobe radius and the system is supposed to be very close to the onset of mass transfer, which is reflected by $t_{\text{sd}} = 0$ within the accuracy of our calculations. Clearly, SDSS J0052-0053 may be a detached CV in the period gap, or a pre-CV that has almost completed its

PCEB lifetime. To estimate the probability for SDSS J0052–0053 being either a period-gap CV or a PCEB close to entering for the first time a semi-detached state, we assume a steady state binary population. In that case, the number of detached CVs in the gap should be roughly equal to the number of CVs above the gap (Kolb 1993). In addition, the number of PCEBs in the gap should be roughly equal to the number of accreting CVs in the gap. According to CV population studies (Kolb 1993), the number of detached CVs in the gap is approximately five times higher than the number of CVs in the gap and the probability for SDSS J0052–0053 being a detached CV in the gap rather than a PCEB is $\sim 80\%$. This result is a simple consequence of the fact that all CVs with donor stars earlier than $\sim M3$ will become detached CVs in the gap while only a rather small fraction of PCEBs, i.e. those with secondary stars of spectral type $\sim M3.5$ – $M4.5$, produces CVs starting mass transfer in the period gap. This is obviously only a rough estimate. A detailed population study by Davis et al. (2008) confirms that the ratio of detached CVs to pre-CVs within the CV period gap is $\sim 4 - 13$, depending on different assumptions of the common envelope ejection efficiency, initial mass ratio distributions, and magnetic braking laws.

7 DISCUSSION

As outlined in the introduction, despite some recent progress our understanding of the CE phase is still very limited. The classical α prescription (Webbink 1984) that is based on a simple energy equation seems to be unable to explain the observed existence of double white dwarfs with stellar components of comparable masses and rather long orbital periods (see Webbink 2007, for more details). This disagreement motivated Nelemans et al. (2000) to develop an alternative prescription based on the conservation of angular momentum, the so-called γ algorithm. Binary population synthesis codes based on the α prescription as well as those assuming the γ algorithm predict the existence of a significant number of PCEBs with orbital periods longer than a day. Using the α mechanism, Willems & Kolb (2004) calculated the expected period distribution of the present-day WDMS binaries in the Galaxy at the start of the WDMS binary phase. Their Fig. 10 clearly shows that the predicted PCEB distribution peaks around $P_{\text{orb}} \sim 1$ day, but also has a long tail of systems with up to ~ 100 d. The γ algorithm, on the other hand, predicts an increase of the number of PCEBs with increasing orbital period up to $P_{\text{orb}} \gtrsim 100$ days, i.e. the γ prescription predicts the existence of even more long orbital period ($P_{\text{orb}} > 1$ day) PCEBs (see Nelemans & Tout 2005; Maxted et al. 2007).

We have measured a total number of nine orbital periods along this work and the recently published paper by Schreiber et al. (2008). All of them have short orbital periods of less than a day. Radial velocity variations are much easier to identify in short orbital period systems, so our sample is expected to be biased towards shorter orbital periods. The crucial question is whether our observational finding, the paucity of PCEBs with $P_{\text{orb}} > 1$ d, is whether the result of that bias, or whether it reflects an intrinsic feature of the PCEB population. To answer this question we performed the following analysis. First, we car-

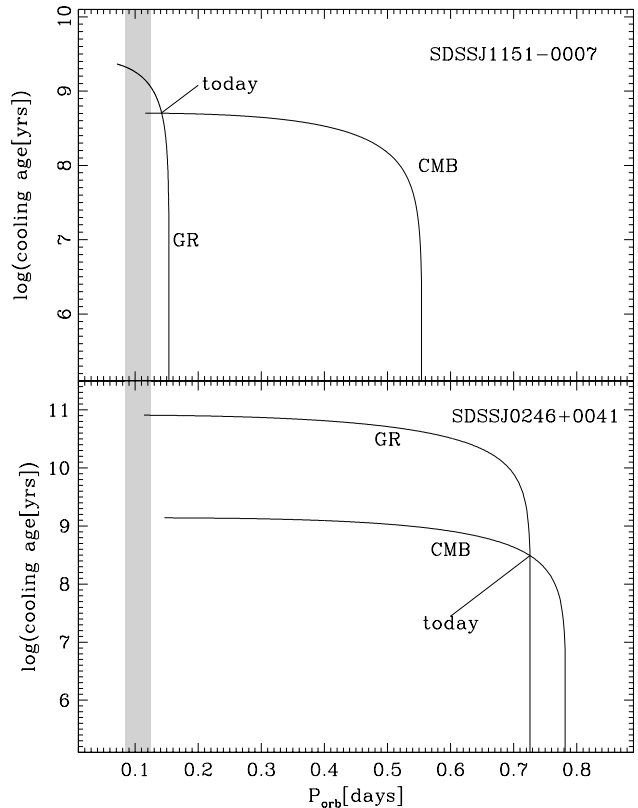


Figure 6. The predicted evolution of two PCEBs. The orbital period gap observed in the orbital period distribution of CVs is shaded. As the secondary masses of SDSS J1151–0007 and SDSS J0246+0041 are close to the fully convective boundary, we calculated the evolution assuming classical magnetic braking (CMB) and assuming only gravitational radiation (GR). Obviously, the calculated orbital periods at the end of the CE phase (P_{CE}), the evolutionary time scale, and the expected zero-age CV orbital period (P_{sd}) differ significantly.

ried out Monte-Carlo simulations similar to those presented in Schreiber et al. (2008)² but assuming a resolution of 15 km/s, corresponding to the typical error in the radial velocity measurements from SDSS spectra. Clearly, as shown in Fig. 7, the bias towards short orbital period systems is larger due to the lower resolution of the SDSS spectra and, as a consequence, radial velocity variations in multiple SDSS spectra of systems with $P_{\text{orb}} > 10$ days are more difficult to detect. However, the probability to detect 3σ radial velocity variations for systems in the orbital period range of $P_{\text{orb}} \sim 1 - 10$ days still is $\sim 20 - 40\%$. Second, we assumed a uniform orbital period distribution and integrated the 3σ -detection probability (lowest dotted line) for systems with $P_{\text{orb}} \leq 1$ day and those with $10 \text{ days} > P_{\text{orb}} > 1$ day. In other words, we assume that there is no decrease for 10 days $P_{\text{orb}} > 1$ day and calculate the total detection probability for 10 days $> P_{\text{orb}} > 1$ day and $P_{\text{orb}} \leq 1$ day. We find that if there was indeed no decrease, the fraction of PCEBs with

² In Schreiber et al. (2008, their Fig. 8) we underestimated the detection probability. Therefore, the correct detection probability for a resolution of 6 km/s as given in Fig. 7 is higher than our previous estimates.

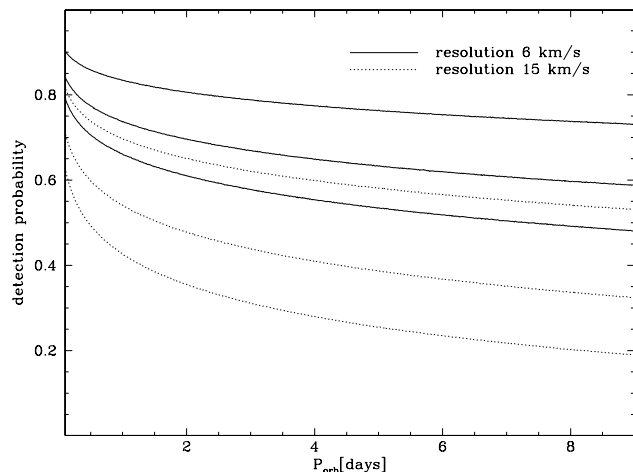


Figure 7. Monte-Carlo simulations of the detection probability of significant radial velocity variations assuming measurement accuracy of 6 km s^{-1} , corresponding to our previous VLT/FORS observations (Schreiber et al. 2008) 15 km/s , as appropriate for the SDSS spectra (Rebassa-Mansergas et al. 2007). The three lines correspond to 1, 2, or 3σ significance of the radial velocity variation. Clearly, even the PCEB identification based on multiple SDSS spectra should be sensitive to PCEBs with orbital periods of $\sim 1 - 10$ days.

$P_{\text{orb}} > 1$ day in our sample should be $\sim 84\%$ and the number of PCEBs with $P_{\text{orb}} > 1$ day among our nine systems should be $\sim 7.6 \pm 2.8$. The result of our observations, i.e. no system with $P_{\text{orb}} > 1$ day among nine PCEBs disagrees with the hypothesis (i.e. there is no decrease) by 2.7σ . This indicates that the measured lack of PCEBs with $P_{\text{orb}} > 1$ day might indeed be a feature of the intrinsic population of PCEBs.

How do our results for PCEBs from SDSS compare with the sample of all known PCEBs? Figure 8 shows in gray the orbital period distribution of all 41 known PCEBs consisting of a M or K-star plus a white dwarf from the latest version of the Ritter & Kolb (2003) catalogue (V7.9), including also the seven new periods from this paper, and the new recent discovery by Steinfadt et al. (2008). As we are interested in analysing the bias of the sample towards shorter orbital periods in the context of detection probability, we superimpose in black a subsample of ten SDSS PCEBs, identified from radial velocity snapshots of SDSS WDMS, representing a homogenous selection mechanism (seven from the current paper, two from Schreiber et al. 2008, one [SDSS J112909.50+663704.4] from Raymond et al. 2003). So far, the period distributions of the two subsets seem very similar, with a steep decrease of the number of systems at $P_{\text{orb}} \sim 1$ day. The total sample of PCEBs contains only six systems with orbital periods larger than one day ($\sim 15\%$ of the entire sample). This suggests that the number of PCEBs decreases for $P_{\text{orb}} > 1$ day, implying that the γ algorithm in its present form might not be an adequate description of the CE phase, and that the common envelope efficiency in the energy equation used in the α prescription is perhaps smaller than assumed previously (lower efficiencies lead to stronger shrinkage of binary separations). However, one should bear in mind that the previously known PCEBs have been discovered by various methods, and therefore do not form a representative sample (see Schreiber & Gänsicke

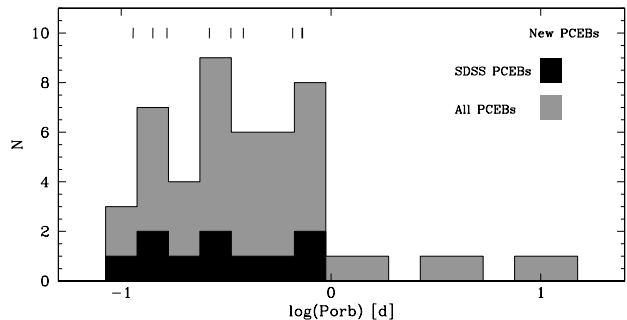


Figure 8. The period distribution of 41 PCEBs from the Ritter & Kolb (2003) (V7.9) catalogue containing a white dwarf plus M or K companion star (gray). The 7 systems studied in this work and the recent PCEB discovery SDSS J143547.87+373338.5 (Steinfadt et al. 2008) are also included. In black is shown a subsample of SDSS PCEBs obtained from RV variation studies. Both subsamples illustrate a clear lack of systems at orbital periods greater than 1 day. The 7 new systems from this work and the two systems in Schreiber et al. (2008) are indicated as tick marks in the top of the figure.

2003, for details). The sample of PCEBs selected in a homogeneous way from the SDSS is still small, and the current sample of WDMS binaries from SDSS involves some selection effects, too (Schreiber et al. 2007), impeding a definite conclusion at this point. However, work is underway to enlarge the parameter space of the SDSS WDMS binaries in terms of ages and secondary star masses (Schreiber et al. 2007), to increase the number of PCEBs with orbital period measurements, and to model the remaining selection effects, paving the way for a more quantitative assessment of CE and post-CE evolution.

8 CONCLUSIONS

We have presented a study of 11 PCEB previously identified candidates, and measured the orbital periods of six and one of them from their Na I doublet radial velocity variations and its differential photometry, respectively. Combining the K_{sec} velocity amplitudes with the results from spectroscopic decomposition/fitting of their SDSS spectra, we constrained the binary parameters of the seven systems for which we could determine orbital periods. No radial velocity variations were detected for three PCEB candidates, suggesting that they may be wide binaries. We revisited the PCEB candidate selection of Rebassa-Mansergas et al. (2007), and conclude that candidates with low amplitude velocity variations, noisy SDSS spectra, and radial velocity shifts that only show up in the $H\alpha$ emission line definitely need additional follow-up spectroscopy for the confirmation/rejection of their PCEB nature. Finally, we have had a first look at the period distribution of PCEBs from SDSS identified from radial velocity snapshots of SDSS WDMS binaries, and noted that none of the ten systems published so far have an orbital period > 1 d. Using a Monte-Carlo simulation, we demonstrated that our method of finding PCEBs should be efficient also for systems with periods > 1 d, and that, subject to small number statistics, it appears that the PCEB period distribution peaks at $P_{\text{orb}} < 1$ d. This is in agree-

ment with the period distribution of the previously known PCEBs, which represents a heterogeneous mix of systems identified by various different methods. In contrast, current binary population models predict a large number of PCEBs with orbital periods > 1 day in clear disagreement with the currently observed sample. Additional effort is needed to improve the size of the sample of known PCEBs, as well as to fully model its selection effects, but with more than 1000 SDSS WDMS binaries to draw from, the outlook for more quantitative tests of CE evolution seem promising.

ACKNOWLEDGEMENTS.

ARM was supported by a STFC-IAC studentship. MRS acknowledges support from FONDECYT (grant 1061199), DIPUV (project 35), and the Center of Astrophysics in Valparaíso (CAV). ANGM, AST, RSC, JV were supported by the DLR under grant 50OR0404. AST acknowledges support by the DFG grant Schw536/20-1. We thank the referee, John Thorstensen for providing comments that helped improving the paper.

Based on observations collected at the European Organisation for Astronomical Research in the Southern Hemisphere, Chile, under programmes 079.D-0531 and 080.D-0407; at the Centro Astronómico Hispano Alemán at Calar Alto, operated jointly by the Max-Planck Institut für Astronomie and the Instituto de Astrofísica de Andalucía; at the WHT, which is operated on the island of La Palma by the Isaac Newton Group in the Spanish Observatorio del Roque de los Muchachos of the Instituto de Astrofísica de Canarias; and at the 1.2-m telescope, located at KryoneriKorinthias, and owned by the National Observatory of Athens, Greece. This paper includes data gathered with the 6.5m Magellan Telescopes located at Las Campanas Observatory, Chile.

REFERENCES

- Adelman-McCarthy, J. K., et al., 2008, *ApJS*, 175, 297
Andronov, N., Pinsonneault, M., Sills, A., 2003, *ApJ*, 582, 358
Aungwerojwit, A., Gänsicke, B. T., Rodríguez-Gil, P., Hagen, H.-J., Giannakis, O., Papadimitriou, C., Allende Prieto, C., Engels, D., 2007, *A&A*, 469, 297
Bertin, E., Arnouts, S., 1996, *A&AS*, 117, 393
Cardini, D., Cassatella, A., 2007, *ApJ*, 666, 393
Chabrier, G., Gallardo, J., Baraffe, I., 2007, *A&A*, 472, L17
Davis, P. J., Kolb, U., Willems, B., Gänsicke, B. T., 2008, *ArXiv e-prints*, 805
Dewi, J. D. M., Tauris, T. M., 2000, *A&A*, 360, 1043
Eggleton, P. P., 1983, *ApJ*, 268, 368
Eibe, M. T., 1998, *A&A*, 337, 757
Gänsicke, B. T., Araujo-Betancor, S., Hagen, H.-J., Harlaftis, E. T., Kitsionas, S., Dreizler, S., Engels, D., 2004, *A&A*, 418, 265
Howell, S. B., Nelson, L. A., Rappaport, S., 2001, *ApJ*, 550, 897
Iben, I. J., Livio, M., 1993, *PASP*, 105, 1373
Kawka, A., Vennes, S., 2003, *AJ*, 125, 1444
Kolb, U., 1993, *A&A*, 271, 149
Livio, M., Soker, N., 1988, *ApJ*, 329, 764
Marsh, T. R., 1989, *PASP*, 101, 1032
Marsh, T. R., Robinson, E. L., Wood, J. H., 1994, *MNRAS*, 266, 137
Maxted, P. F. L., Napiwotzki, R., Marsh, T. R., Burleigh, M. R., Dobbie, P. D., Hogan, E., Nelemans, G., 2007, in *Napiwotzki & Burleigh (2007)*, p. 471, p. 471
Mullan, D. J., MacDonald, J., 2001, *ApJ*, 559, 353
Napiwotzki, R., Burleigh, R., eds., 2007, 15th European Workshop on White Dwarfs, ASP Conf. Ser. 372
Nelemans, G., Tout, C. A., 2005, *MNRAS*, 356, 753
Nelemans, G., Verbunt, F., Yungelson, L. R., Portegies Zwart, S. F., 2000, *A&A*, 360, 1011
Orosz, J. A., Wade, R. A., Harlow, J. J. B., Thorstensen, J. R., Taylor, C. J., Eracleous, M., 1999, *AJ*, 117, 1598
Paczynski, B., 1976, in *Eggleton, P., Mitton, S., Whelan, J., eds., IAU Symp. 73: Structure and Evolution of Close Binary Systems*, D. Reidel, Dordrecht, p. 75
Politano, M., Weiler, K. P., 2006, *ApJ Lett.*, 641, L137
Politano, M., Weiler, K. P., 2007, *ApJ*, 665, 663
Rappaport, S., Joss, P. C., Verbunt, F., 1983, *ApJ*, 275, 713
Raymond, S. N., et al., 2003, *AJ*, 125, 2621
Rebassa-Mansergas, A., Gänsicke, B. T., Rodríguez-Gil, P., Schreiber, M. R., Koester, D., 2007, *MNRAS*, 382, 1377
Ricker, P. M., Taam, R. E., 2008, *ApJ Lett.*, 672, L41
Ritter, H., Kolb, U., 2003, *A&A*, 404, 301
Sandquist, E. L., Taam, R. E., Burkert, A., 2000, *ApJ*, 533, 984
Scargle, J. D., 1982, *ApJ*, 263, 835
Schreiber, M., Nebot Gomez-Moran, A., Schwöpe, A., 2007, in *Napiwotzki & Burleigh (2007)*, p. 459, p. 459
Schreiber, M. R., Gänsicke, B. T., 2003, *A&A*, 406, 305
Schreiber, M. R., Gänsicke, B. T., Southworth, J., Schwöpe, A. D., Koester, D., 2008, *A&A*, 484, 441
Schwarzenberg-Czerny, A., 1996, *ApJ Lett.*, 460, L107
Silvestri, N. M., et al., 2007, *AJ*, 134, 741
Southworth, J., Gänsicke, B. T., Marsh, T. R., de Martino, D., Hakala, P., Littlefair, S., Rodríguez-Gil, P., Szkody, P., 2006, *MNRAS*, 373, 687
Steinfadt, J. D. R., Bildsten, L., Howell, S. B., 2008, *ApJ Lett.*, 677, L113
Stoughton, C., et al., 2002, *AJ*, 123, 485
Taam, R. E., Ricker, P. M., 2006, *astro-ph/0611043*
Tappert, C., Gänsicke, B. T., Schmidtobreick, L., Aungwerojwit, A., Mennickent, R. E., Koester, D., 2007, *A&A*, 474, 205
Vennes, S., Thorstensen, J. R., Polonski, E. F., 1999, *ApJ*, 523, 386
Verbunt, F., Zwaan, C., 1981, *A&A*, 100, L7
Wade, R. A., Horne, K., 1988, *ApJ*, 324, 411
Webbink, R. F., 1984, *ApJ*, 277, 355
Webbink, R. F., 2007, *ArXiv e-prints*, 704
Willems, B., Kolb, U., 2004, *A&A*, 419, 1057
Wood, M. A., 1995, in *Koester, D., Werner, K., eds., White Dwarfs*, no. 443 in LNP, Springer, Heidelberg, p. 41
York, D. G., et al., 2000, *AJ*, 120, 1579